Biochimica et Biophysica Acta 1807 (2011) 755–767

Contents lists available at ScienceDirect

Biochimica et Biophysica Acta

journal homepage: www.elsevier.com/locate/bbabio

Modeling cancer glycolysis ☆

Alvaro Marín-Hernández, Juan Carlos Gallardo-Pérez, Sara Rodríguez-Enríquez, Rusely Encalada, Rafael Moreno-Sánchez *, Emma Saavedra *

Departamento de Bioquímica, Instituto Nacional de Cardiología, México D.F. 14080, Mexico

ARTICLE INFO

Article history:
Received 4 June 2010
Received in revised form 1 November 2010
Accepted 9 November 2010
Available online 24 November 2010

Keywords:
Metabolic control analysis
Flux-control coefficient
Hexokinase
Phosphofructokinase type 1
Glucose transporter
Combined therapy

ABSTRACT

Most cancer cells exhibit an accelerated glycolysis rate compared to normal cells. This metabolic change is associated with the over-expression of all the pathway enzymes and transporters (as induced by HIF-1α and other oncogenes), and with the expression of hexokinase (HK) and phosphofructokinase type 1 (PFK-1) isoenzymes with different regulatory properties. Hence, a control distribution of tumor glycolysis, modified from that observed in normal cells, can be expected. To define the control distribution and to understand the underlying control mechanisms, kinetic models of glycolysis of rodent AS-30D hepatoma and human cervix HeLa cells were constructed with experimental data obtained here for each pathway step (enzyme kinetics; steady-state pathway metabolite concentrations and fluxes). The models predicted with high accuracy the fluxes and metabolite concentrations found in living cancer cells under physiological O_2 and glucose concentrations as well as under hypoxic and hypoglycemic conditions prevailing during tumor progression. The results indicated that HK ≥ HPI > GLUT in AS-30D whereas glycogen degradation ≥ GLUT > HK in HeLa were the main flux- and ATP concentration-control steps. Modeling also revealed that, in order to diminish the glycolytic flux or the ATP concentration by 50%, it was required to decrease GLUT or HK or HPI by 76% (AS-30D), and GLUT or glycogen degradation by 87–99% (HeLa), or decreasing simultaneously the mentioned steps by 47%. Thus, these proteins are proposed to be the foremost therapeutic targets because their simultaneous inhibition will have greater antagonistic effects on tumor energy metabolism than inhibition of all other glycolytic, non-controlling, enzymes. This article is part of a Special Issue entitled Bioenergetics of Cancer.

1. Introduction

Cancer treatments are mostly based on the higher susceptibility of tumor cells to damage caused by radiation and chemotherapy compared to normal non-proliferating cells. However, their severe side effects in the patients and the frequent lack of tumor response (due to inherent or acquired resistance) make necessary the development of novel therapeutic strategies to fight this deadly disease. Hence, the identification of the main differences at the molecular and functional levels between normal and tumor cells is essential in the search for new therapeutic targets.

In this regard, the most frequent metabolic alteration in the majority of tumor cells is a higher glucose consumption (with a concomitant higher lactate production) compared to normal cells [reviewed in 1,2]. The accelerated glycolysis rate can provide the required glycolytic intermediary precursors for DNA, protein and lipid synthesis necessary to sustaining the active proliferation of tumor cells. Moreover, glycolysis can be the main energy-generating pathway under conditions where mitochondrial function is absent or diminished such as in the initial non-vascular stages of tumor progression where hypoxic conditions prevail.

The cellular mechanisms involved in augmenting the glycolytic flux are the simultaneous increased transcription of the genes encoding glycolytic enzymes and transporters in processes mediated by the hypoxia-inducible factor 1α (HIF1α) and other oncogenes [reviewed in 3–5]. The higher transcription coupled to higher translation are responsible for the increased contents and activities of glycolytic

Abbreviations: AlaTA, alanine transaminase; ALDO, fructose 1,6 bisphosphate aldolase; C^M_{Ei}, concentration control coefficient; DHAP, dihydroxyacetone phosphate; ENO, enolase; Ery4P, erythrose-4-phosphate; FBP, fructose-1,6-bisphosphate; F6P, fructose-6-phosphate; F2,6BP, fructose-2,6-bisphosphate; C^J_{Ei}, Flux control coefficient of enzyme i on flux J; GAPDH, glyceraldehyde-3-phosphate dehydrogenase; G1P, glucose-1-phosphate; G3P, glyceraldehyde-3-phosphate; G6P, glucose-6-phosphate; G6PDH, glucose-6-phosphate dehydrogenase; GLUT, glucose transporter; αGPDH, α-glycerophosphate dehydrogenase; HK, hexokinase; HPI, hexose-6-phosphate isomerase; LDH, lactate dehydrogenase; MPM, mitocondrial pyruvate metabolism; PEP, phosphoenolpyruvate; PFK-1, phosphofructokinase type 1; PGAM, 3-phosphoglycerate mutase; PGK, 3-phosphoglycerate kinase; PGM, phosphoglucomutase; PPP, pentose phosphate pathway; Pyr, pyruvate; PYK, pyruvate kinase; Rib5P, ribose 5-phosphate; TPI, triosephosphate isomerase; TA, transaldolase; TK, transketolase; Xy5P, xylulose 5-phosphate; 2PG, 2-phosphoglycerate; 3PG, 3-phosphoglycerate; 6PG, 6-phosphogluconate; 3PGDH, 3 phosphoglycerate dehydrogenase

☆ This article is part of a Special Issue entitled Bioenergetics of Cancer.

* Corresponding authors. Departamento de Bioquímica, Instituto Nacional de Cardiología, Juan Badiano No. 1, Col. Sección XVI, Tlalpan, México D.F. 14080, Mexico. Tel.: +52 555573 2911x1298.

E-mail addresses: rafael.moreno@cardiologia.org.mx (R. Moreno-Sánchez), emma_saavedra2002@yahoo.com (E. Saavedra).

0005-2728/$ – see front matter © 2010 Elsevier B.V. All rights reserved.
doi:10.1016/j.bbabio.2010.11.006

enzymes and transporters which result in an increased pathway flux. HIF-1α induces the expression of specific glycolytic protein isoforms (*i.e.*, GLUT1, GLUT3, HKI and II, PFK-L, ALDO-A and C, PGK1, ENOalpha- PYK-M2, LDH-A and PFKFB-3) which are not usually found together in normal cells. Some of these isoforms show lower sensitivity to physiological inhibitors and lower affinity for products, thus favoring a higher forward (glycolytic) rate compared to normal cells [reviewed in 5].

Because of its relevance on tumor metabolism, inhibition of glycolytic flux has been considered an alternative strategy for cancer treatment [reviewed in 6]. However, since both tumor and non-tumor cells contain a similar set of glycolytic enzymes, it is mandatory to find striking differences in pathway control so that the tumor enzyme(s) with the highest control be different to those in normal cells. Perhaps some of the side-effects induced by anticancer glycolytic drugs have derived from their lack of specificity, targeting both cancer and non-cancer cells.

Metabolic Control Analysis (MCA) has shown that the control of a pathway flux or a metabolite concentration is distributed in different degrees among all the pathway enzymes, thus circumventing the misleading and qualitative concept of the "rate-limiting step" and moving into a quantitative analysis of the control of metabolic pathways [7–9]. MCA allows for the quantitative determination of the degree of control that each enzyme has over the pathway flux and the intermediary concentrations, namely, the flux control coefficient (C^J_{Ei}) and the concentration control coefficient (C^M_{Ei}), respectively, where *J* is flux, *M* is a metabolite concentration and *Ei* is a pathway enzyme. A practical definition of these coefficients is the percentage of change in flux or metabolite concentration when a 1% change in a pathway enzyme activity is attained.

By applying different experimental approaches such as elasticity analysis and metabolic modeling, the control distribution of a metabolic pathway can be determined [7,8]. The advantages of the elasticity analysis strategy are that it allows determining of the control distribution in living cells, and that it is not required to know the complete set of the kinetic parameters of the pathway enzymes. In a previous work, elasticity analysis was applied to glycolysis in rodent AS-30D hepatoma [10]. The results indicated that the pathway was mainly controlled by the glucose transporter (GLUT) *plus* hexokinase (HK) segment (71%; *i.e.*, $C^J_{GLUT+HK}=0.71$), with lesser control attained by phosphofructokinase 1 (PFK-1) ($C^J_{PFK\text{-}1}=0.06$). The rest of the control ($C^J_{Ei}=0.25$) resided within the aldolase (ALDO) to lactate dehydrogenase (LDH) segment [10].

As elasticity analysis relies on quantifiable small changes in pathway intermediary concentrations, thus dividing the analyzed pathway in segments, this approach determines control coefficients only by group of enzymes. Hence, in our previous study it was not possible to define in the glucose-6-phosphate producing segment which individual step, GLUT, HK or even glycogen degradation, was exerting the main flux control.

Kinetic modeling of a metabolic pathway integrates all available information (detailed kinetic properties of the individual enzymes and transporters, metabolite concentrations and pathway fluxes) into a functional, cross-talking network that attempts to simulate what occurs in the intracellular milieu [reviewed in 8,11]. Thus, the aim of kinetic modeling is to construct a model able to predict the fluxes and concentrations found in a cell under different specific metabolic steady-states. Validated models allow for the identification of the mechanisms by which a metabolic pathway is controlled and also provide the individual C^J_{Ei} and C^M_{Ei} for each pathway step. By extending this approach to normal (host, normal cells) and pathologic systems (tumor cells, parasites) the enzymes and transporters with the highest control in the latter and low control in the former can be identified and hence proposed as the best and most adequate therapeutic targets [8,12].

In the present work, we report on the kinetic modeling of glycolysis in rat AS-30D hepatoma and in human HeLa tumor cells under normoxic and physiological glucose concentration conditions characteristics of *in vitro* culture experimentation and under hypoxic and glucose deprivation conditions prevailing during tumor formation. The results indicated that in the evaluated conditions, the flux control was shared mainly among HK≥HPI>GLUT in AS-30D cells and glycogen degradation≥GLUT>HK in HeLa cells. Further modeling analysis showed that simultaneous inhibition of these controlling steps has greater negative effects on tumor glycolysis than inhibition of non-controlling reactions.

2. Experimental procedures

2.1. Enzymes and chemicals

HK, G6PDH, HPI, ALDO, GAPDH, αGPDH, αGPDH/TPI, PYK/LDH, LDH, G1P, G6P and F6P were purchased from Roche (Manheim, Germany). Recombinant enzymes ENO, PPi-PFK and PGK from *Entamoeba histolytica* were those previously described [13]. Glucose (Glu), 6PG, FBP, G3P, 2PG, 3PG, PEP, Pyr, Rib5P, Ery4P, Xy5P, ATP, ADP, GTP, DTT, cysteine, NADH, NAD^+, $NADP^+$, 6PGDH, amyloglucosidase, TK, TA, $MgCl_2$ and lyophilized ALDO, αGPDH and TPI were from Sigma (St Louis, MO, USA). DHAP was from Fluka (Buchs, Switzerland). Mops and Hepes were from Research Organics (Cleveland, Ohio, USA). Potato PPi-PFK was purified as previously described [14].

2.2. Enzyme activities

Clarified cytosolic extracts from AS-30D and HeLa cells were prepared as previously described [10]. Glycolytic enzyme activities and affinity constants were determined for the forward (glycolytic) and reverse (gluconeogenic) reactions in 50 mM Mops buffer pH 7.0 (assay buffer) at 37 °C by following the $NAD(P)^+$ reduction or NAD(P)H oxidation at 340 nm in a spectrophotometer (Agilent; Santa Clara, CA, USA). Standard kinetic assays were initially used [15,16], but the substrate concentrations were always adjusted to ensure they were saturating for the tumor cell enzymes. The activities were determined under initial-rate conditions; the reactions were started by adding the specific substrates and the absorbance baseline in the absence of one substrate was always subtracted. PGM, AlaTA and 3PGDH activities were determined by standard assays [15,16]. TK and TA were measured according to [17].

The Ery4P, FBP and 6PG inhibition on HPI in the forward direction was determined in assay buffer containing 5 mM $MgCl_2$, 1 mM PPi, 0.15 mM NADH, 1 U *E. histolytica* PPi-PFK, 0.36 U ALDO, 9 U TPI, 3.1 U αGPDH and 0.003–0.014 mg of cytosolic extract *plus* 13.8–28 μM Ery4P, 30–60 μM 6PG or 3–10 mM FBP. The reaction was started by adding G6P (0.1–7 mM). HPI inhibition was also evaluated in the reverse reaction in assay buffer containing 1 mM $NADP^+$, 2 U G6PDH, and 13–55 μM Ery4P, 40–90 μM 6PG or 3–10 mM FBP, and 0.001–0.01 mg of extract. The reaction was started with the addition of 0.05–10 mM F6P.

PFK-1 activity was determined according to [10] with lyophilized (ammonium-free) coupling enzymes.

2.3. Steady-state metabolite concentrations

AS-30D hepatoma cells were collected from rat ascites fluid. HeLa cells were cultured under normoxic (95% air–5% CO_2) conditions in Dulbecco-MEM medium at 37 °C as previously described [18]. For hypoxic conditions, HeLa cells were initially grown under normoxia; then at 75–90% confluency, cells were subjected for 24 h to 0.1–0.2% oxygen in a humidified hypoxia incubator chamber (Billups-Rothenberg, California, USA) as described before [19].

The experimental protocol to attain glycolytic flux under steady-state conditions was described elsewhere [10]. Briefly, the cells were harvested, washed and re-suspended in Krebs–Ringer medium (125 mM NaCl, 5 mM KCl, 1 mM $MgCl_2$, 1.4 mM $CaCl_2$, 1 mM KH_2PO_4, and 25 mM Hepes, pH 7.4). The cells were incubated at 37 °C under orbital shaking; after 10 min, 5 mM glucose (or 1 mM for AS-30D under

low glucose concentration) was added and incubated for another 3 min and the reaction was terminated by perchloric acid (3% v/v, final concentration) extraction.

Glycolytic metabolite concentrations were determined as previously described [10]. The concentrations of NAD^+, G1P, alanine and 6PG were determined in neutralized extracts as described before by using LDH; PGM plus G6PDH; AlaTA plus LDH and 6PGDH, respectively [20]. The Ery4P concentration was determined in 50 mM Hepes, 1 mM EGTA, pH 7.4, *plus* 0.7 mM Xy5P, 5 mM $MgCl_2$, 0.5 mM $NADP^+$, 0.04 mM thiamine pyrophosphate (TPP), 1 U/ml of each HPI and G6PDH, and 0.5 U/ml of TK.

For F2,6BP determination, after the 3 min incubation with glucose, the cells were quickly spun down; the pellet was re-suspended in 25 mM Tris–HCl pH 7.6 and the cells were disrupted by freezing in liquid N_2 and thawing at 37 °C three times. The homogenate was centrifuged at 20,800×*g* for 3 min at 4 °C. The supernatant was alkalinized with NaOH to a final concentration of 0.1 mM and heated at 80 °C for 5 min. The sample was centrifuged and the supernatant was neutralized with acetic acid. F2,6BP was determined by using potato PPi-PFK as described elsewhere [14].

For determination of the total intracellular Pi, cells were incubated for 3 min with glucose, and then a sample of 1 ml was withdrawn and centrifuged at 800×*g* for 30 s. The cell pellet was washed three times with saline (0.9% NaCl) and re-suspended in 1 ml of the same solution. The cellular suspension was divided into two; the first sample was centrifuged at 20,800×*g* for 1 min and the supernatant was recovered whereas the second sample was extracted with perchloric acid (3% v/v final volume), centrifuged for 5 min as above and the supernatant was recovered. Pi was determined in the supernatants as described elsewhere [21]. The intracellular total Pi content was calculated from the difference between the Pi present in the first supernatant (extracellular Pi) from that in the second supernatant (extracellular plus intracellular Pi). The concentration of cytosolic free Pi was calculated assuming that only 53% of the total content was in its free form, as previously determined in hepatocytes [22].

2.4. Metabolic fluxes

For the determination of the glycogen synthesis and degradation fluxes, AS-30D cells (15 mg protein/ml) were pre-incubated at 37 °C for 10 min in Krebs–Ringer medium. Then, an aliquot was withdrawn (t = 0) and 5 mM glucose was added to the cellular suspension and kept under the same conditions. Aliquots were taken at 10 and 30 min, immediately centrifuged, and the cellular pellet was frozen in liquid N_2 and kept at −70 °C until use. The pellet was further re-suspended in 0.3 ml of 30% KOH and heated for 30 min at 90 °C; afterwards, the sample was mixed with 0.1 ml 6% Na_2SO_4 and 0.9 ml 100% ethanol and centrifuged at 20,800 *g* for 5 min. The pellet was washed once with 1 ml of 80% ethanol and let dry at room temperature. Then, the pellet was re-suspended in 0.5 ml 0.2 M acetate buffer pH 4.8 *plus* 5 U amyloglucosidase and incubated for 1 h at 37 °C. Glucose units derived from glycogen breakdown were determined by enzymatic analysis by using HK and G6PDH [20] and reported as nmol of glucose equivalents. After the addition of glucose, the glycogen degradation rate was calculated from the difference of glucose equivalents in glycogen from the 10 min *minus* 0 min incubation, whereas the glycogen synthesis rate was calculated from the difference of glucose equivalents in glycogen from the 30 min *minus* 10 min incubation. For HeLa cells, glycogen synthesis and degradation rates were determined in cells (5–7 mg protein) incubated with and without glucose, respectively. The samples were taken at 0 and 3 min and treated as described above.

For the pentose phosphate pathway (PPP) flux, AS-30D cells were incubated as described above for glycogen metabolism analysis. After glucose addition, samples were withdrawn at 2, 4 and 6 min and immediately precipitated with perchloric acid, centrifuged and the supernatant neutralized. The 6PG content was determined in the neutralized extracts by using a 6PGDH assay [20]. The rate was calculated from the differences in 6PG concentrations at different time points.

The pyruvate consumption rate by mitochondria (mitochondrial pyruvate metabolism; MPM) was estimated from the total cellular oxygen consumption rate *minus* that in the presence of 5 μM oligomycin, and assuming that the main substrate consumed by mitochondria was the endogenous pool of pyruvate generated by the cells (equivalent to 4 mg cellular protein) incubated with 5 mM glucose for 5 min. For the calculations it was assumed that 6 mol of O_2 (12 atoms oxygen) are consumed *per* mol of completely oxidized glucose. It is noted that the MPM flux is the result of the coordinated activities of the pyruvate transporter, pyruvate dehydrogenase complex, Krebs cycle enzymes, respiratory chain complexes, adenine nucleotide translocator, Pi carrier and ATP synthase.

For the majority of the parameters described above (enzyme activities, metabolite concentrations and fluxes) at least two different batches of cells were assayed. The high dispersion in the experimental data is very common when using non-chemostat cultures and when using different batches of cellular cultures. On the other hand, lower dispersions can be certainly obtained by measuring triplicates of one homogeneous cell culture, but such results only represent one independent sampling.

2.5. Construction of the kinetic models

The models were constructed by using the software Gepasi v 3.3 [23] available at the web site http://www.gepasi.org/. Fig. 1 diagrammed the pathway reactions considered in both models. The reactions were written in the program as described in Table S1 and a summary of all the used kinetic parameters is provided in Tables S2, S3, and S4 of supplementary material.

All glycolytic reactions (including those of HK, PFK-1 and PYK) were considered reversible. For most of them, their *Vm* values were determined in cytosolic extracts in the forward and reverse reactions (Table 1) thus avoiding the use of *Keq* values taken from the literature in the rate equations (see below). Since these *Vm* values actually corresponded to those of the enriched cytosolic fractions, these were also experimentally determined in whole cells which were solubilized with 0.02% Triton X-100 to obtain the corresponding *Vm* in total cellular protein units (Table S3); the latter *Vm* values were used in the models.

The kinetic parameters *Vmf*, *Vmr* and *Km* for substrates, products and modulators were all determined under the same conditions of pH (7.0) and temperature (37 °C) (Table 1), whereas those of the glucose transporters were previously determined by our research group [24].

The oxidative and non-oxidative PPP sections, the glycogen synthesis and degradation pathways and the MPM branches were simplified and considered as non-reversible reactions with the constant flux values shown in Table 2. The glycogen metabolism reactions only included the initial substrates and the final products without considering the intermediate reactions catalyzed by PGM. The oxidative PPP section did not include the NADPH production whereas the non-oxidative section only included the reaction catalyzed by TK.

The cellular ATP consuming processes (ATPases) were represented as a mass-action irreversible reaction with an adjusted *k* value of 0.0042. To maintain the pyridine and adenine nucleotide balances, the DHases and adenylate kinase (AK) reactions were used, respectively, with mass-action reversible kinetics whose values were adjusted at $k_1 = 250$ and $k_2 = 1$ and $k_1 = 1$ and $k_2 = 2.26$, respectively. Conserved moieties were [ATP] + [ADP] + [AMP] = 11.3 mM and [NADH] + [NAD^+] = 1.35 mM.

In the pathway modeling, metabolite concentrations were initialized at the values found in the cells (Tables 3 and 4). Fixed metabolite concentrations were used for lactate, glycogen, 6PG, Ery4P, F2,6BP, Pi, citrate and Xy5P at the values shown in Tables 2–4 (summarized in Table S4 of supplementary material) except for Pi, for which only 53% of the total Pi content was assumed to be free Pi [22].

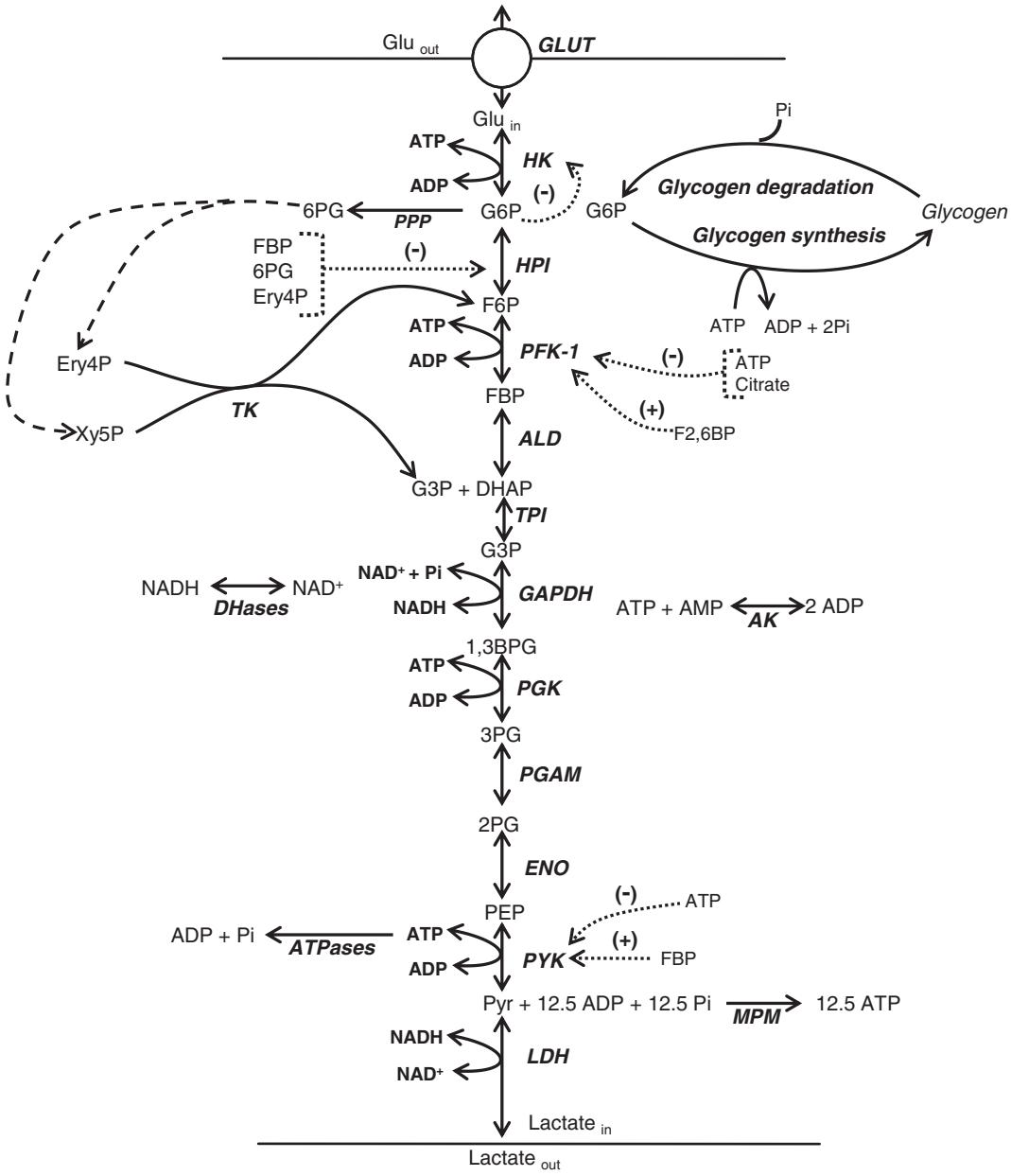

Fig. 1. Pathway reactions included in the kinetic models of glycolysis in AS-30D and HeLa tumor cells. Solid arrows indicate whether reactions are considered non-reversible or reversible in Gepasi; dotted arrows indicate allosteric modulators; dashed arrows indicate PPP existing reactions not included in the model. DHases; NADH consuming enzymes; ATPases, ATP-consuming processes; PPP, pentose phosphate pathway; MPM, mitochondrial pyruvate metabolism. ATP stoichiometry was calculated by using P/O ratios of 2.5 and 1.5 for NADH and $FADH_2$, respectively.

2.6. Rate-equations

The rate-equations used for each reaction are described below.

The kinetics of GLUT was introduced as a monosubstrate reversible Michaelis–Menten equation (Haldane's equation) [25]:

$$v = \frac{Vmf\left([Glu_{out}] - \frac{[Glu_{in}]}{Keq}\right)}{K_{Gluout}\left(1 + \frac{[Glu_{in}]}{K_{Gluin}}\right) + Glu_{out}}$$

in which Glu_{out} and Glu_{in} and K_{Gluout} and K_{Gluin} are the extra- and intra-cellular glucose concentrations and the enzyme's affinity constants (*Km* values), respectively; Keq is the equilibrium constant; and *Vmf* is the maximal velocity in the forward reaction.

The HK rate equation was described as random bi-substrate Michaelis–Menten [25]:

$$v = \frac{\frac{Vmf}{KaKb}\left([A][B] - \frac{[P][Q]}{Keq}\right)}{1 + \frac{[A]}{Ka} + \frac{[B]}{Kb} + \frac{[A][B]}{KaKb} + \frac{[P]}{Kp} + \frac{[Q]}{Kq} + \frac{[P][Q]}{KpKq} + \frac{[A][Q]}{KaKq} + \frac{[P][B]}{KpKb}}$$

in which [A] and [B] represent the substrate concentrations (Glu and ATP, respectively), whereas [P] and [Q] represent the product concentrations (G6P and ADP, respectively). *Ka*, *Kb*, *Kp* and *Kq* represent the enzymes *Km* values for their respective ligands.

The HPI rate equation was introduced as a monoreactant reversible equation with competitive inhibition by Ery4P, 6PG and FBP:

$$v = \frac{Vmf\frac{[G6P]}{K_{G6P}} - Vmr\frac{[F6P]}{K_{F6P}}}{1 + \frac{[G6P]}{K_{G6P}} + \frac{[F6P]}{K_{F6P}} + \frac{[ERY4P]}{K_{ERY4P}} + \frac{[6PG]}{K_{6PG}} + \frac{[FBP]}{K_{FBP}}}$$

Table 1
Kinetic parameters of AS-30D and HeLa glycolytic enzymes and transporter.

Enzyme		AS-30D	HeLa	Enzyme		AS-30D	HeLa
GLUT	Vm_f	0.055[a,e]	0.017[a,e]	GAPDH	Vm_f	1[b]	2[b]
	Km_{Glu}	0.52[a]	9.3[a]		Vm_r	0.9[b]	2.5[b]
HK	Vm_f	0.46[b]	0.06[a]		Km_{G3P}	0.29	0.19
	$K_{m\ Glu}$	0.18[b]	0.1		$Km_{1,3BPG}$	0.02	0.022
	Km_{ATP}	0.99[b]	1.1		Km_{NAD+}	0.08	0.09
	Ki_{G6P}	0.02[c]	0.02[c]		Km_{NADH}	0.004	0.01
HPI	Vm_f	4.9 ± 1.9 (3)	1.2 ± 0.2 (3)		Km_{Pi}	11 ± 1 (3)	29
	Vm_r	3.4 ± 1.1 (6)	2.8 (2)	PGK	Vm_f	27[b]	13[b]
	Km_{G6P}	0.9 ± 0.2 (4)	0.4 ± 0.03 (3)		Vm_r	4.3	3.8
	Km_{F6P}	0.07 ± 0.03 (6)	0.05 (2)		$Km_{1,3DPG}$	0.035	0.079
PFK-1	Vm_f	0.273[d]	0.078[d]		Km_{3PG}	0.12	0.13
	Km_{F6P}	4.6[d]	1.0[d]		Km_{ADP}	0.67	0.04
	Km_{ATP}	0.048[d]	0.021[d]		Km_{ATP}	0.15	0.27
	Ki_{ATP}	1.75[d]	20[d]	PGAM	Vm_f	20[b]	1.4[b]
	Ki_{CIT}	3.9[d]	6.8[d]		Vm_r	1.3	0.53
	Ka_{F26BP}	1.8×10^{-4}[d]	8.4×10^{-4}[d]		Km_{3PG}	0.18 (2)	0.19
ALDO	Vm_f	0.23[b]	0.2[b]		Km_{2PG}	0.04	0.12
	Vm_r	0.18	NM	ENO	Vm_f	0.51[b]	0.36[b]
	Km_{FBP}	0.01	0.009		Vm_r	0.74	0.4
	Km_{G3P}	0.16	NM		Km_{2PG}	0.16	0.038
	Km_{DHAP}	0.08	NM		Km_{PEP}	0.04	0.06
TPI	Vm_f	5.6	5	PYK	Vm_f	6.6[b]	3[b]
	Vm_r	56[b]	42[b]		Km_{PEP}	0.4	0.014
	Km_{DHAP}	1.9	1.6		Km_{ADP}	0.3	0.4
	Km_{G3P}	0.41	0.51	LDH	Vm_f	13.4	11.4
					Vm_r	1.8	NM
					Km_{Pyr}	0.13	0.3
					Km_{Lac}	4.7	NM
					Km_{NAD}	0.07	NM
					Km_{NADH}	0.002	NM

Vm in the forward (Vm_f) and reverse (Vm_r) reactions in U × (mg cytosolic protein)$^{-1}$; *Km* in mM. Values taken from [a][24]; [b][10]; [c][66], [d][Moreno-Sánchez R, Marín-Hernández A, Encalada R and Saavedra E, unpublished results]. [e]*Vm* in U × (mg total cellular protein). The number of independent batches of cells assayed is shown in parentheses; the absence of parenthesis indicates one assayed preparation. NM, not measured.

Table 2
Properties of some glycolytic branches in tumor cells.

	AS-30D	HeLa
Glycogen metabolism		
PGM activity[1]	0.32 ± 0.1 (3)	0.75 ± 0.2 (3)
Km_{G1P}^{3}	NM	0.07
glycogen content[2]	33 ± 30 (5) (26 mM)[c]	171 ± 55 (4) (135 mM)[c]
G1P content[3]	0.08 ± 0.04 (3)	NM
glycogen synthesis flux[4]	2.2 ± 0.3 (3)	2.4 (2)
glycogen degradation flux[4]	1.2 (2)	12 ± 2 (3)
Pentose phosphate pathway		
G6PDH activity[1]	0.05[a]	0.22[a]
6PG content[3]	0.35 ± 0.13 (5)	0.39
PPP flux[4]	0.096 ± 0.03 (3)	NM
TA activity[1]	0.043 ± 0.006 (3)	0.033 (2)
TK activity[1]	0.010 ± 0.001 (3)	0.037
Ery4P content[3]	1 ± 0.3 (3)	0.016[b]
Xyl5P content	NM	0.016[b]
Triglyceride synthesis		
αGPDH activity[1]	ND[a]	ND[a]
Amino acid metabolism		
3PGDH activity[1]	ND	ND
AlaTA activity[1]	0.046 ± 0.022 (3)	0.012 (2)
Alanine content[3]	ND	ND
Mitochondrial pyruvate metabolism		
Flux of pyruvate consumed by mitochondria[4]	1.8 (2)	NM

[1]U (mg cytosolic protein)$^{-1}$; [2]nmol glucose equivalents (mg total cellular protein)$^{-1}$; [3]in mM; [4]nmol min^{-1} (mg total cellular protein)$^{-1}$. Values were taken from [a][10] and [b][39]. [c]The glycogen concentration was calculated by assuming that 1.8 mg total cellular protein has a volume of 2.28 μl [38]. The values are mean ± SD and the number of independent batches of cells assayed is shown in parentheses: the absence of parenthesis indicates one preparation assayed. NM, not measured; ND, not detected.

Table 3
Glycolytic flux and intermediary concentrations obtained *in vivo* (cells) and by *in silico* modeling for AS-30D cells.

Metabolite	5 mM glucose		1 mM glucose[c]	
	In vivo[a]	Model	*In vivo*[b]	Model
Glu_{in}	6.2 ± 1	3.4	NM	0.8
G6P	5.3 ± 2.6	6.5	2 ± 0.5 (4)	3.0
F6P	1.5 ± 0.7	0.03	0.7 ± 0.2 (4)	0.016
FBP	25 ± 7.6	5.2	0.6 ± 0.3 (3)	0.36
DHAP	10 ± 2.3	14	1 ± 0.3 (3)	4.0
G3P	0.9 ± 0.4	0.3	0.38 (2)	0.09
1,3BPG	ND	0.01	NM	0.002
3PG	ND	0.01	NM	0.005
2PG	ND	0.04	NM	0.016
PEP	0.1 ± 0.02	0.003	NM	0.001
Pyr	2.1 ± 1	0.84	0.72 (2)	0.78
lactate	27 ± 11	Fixed	NM	Fixed
F2,6BP ($\times10^{-3}$)	6 ± 1(3)[b]	Fixed	NM	Fixed
citrate	1.7 ± 0.7	Fixed	NM	Fixed
ATP	5.6 ± 1.2	7.9	6 (2)	4.9
ADP	2.4 ± 0.7	2.1	1.5 (2)	2.9
AMP	3.3 ± 1.4	1.3	NM	3.9
Pi	4.8 ± 1.9 (3)[b]	Fixed[d]	5 (1)[b]	Fixed[d]
NADH	NM	0.005	NM	0.005
NAD^+	1.3 ± 0.5 (4)[b]	1.34	NM	1.34
Glycolytic flux	21 ± 9	29	10.5 (2)	14

Metabolite concentrations in mM; flux in nmol lactate min^{-1} (mg cellular protein)$^{-1}$. Values taken from [a][10]. [b]This study. [c]In the model, when this condition was simulated, Glu_{out} concentration and glycogen synthesis flux were fixed at values of 1 mM and 1 nmol min^{-1} (mg of cellular protein)$^{-1}$, respectively. [d]53% of the total Pi concentration shown was assumed to be free Pi [22] which was used for pathway modeling. Figures in parentheses indicate number of independent cellular extracts assayed. NM, not measured; ND, not detected. Fixed values in the model were at those experimentally determined in cells.

Table 4
Glycolytic flux and intermediary concentrations obtained *in vivo* (cells) and by *in silico* modeling for HeLa cells.

Metabolite	Normoxia		Hypoxia[c]	
	In vivo[a]	Model	*In vivo*[b]	Model
Glu_{in}	NM	0.61	NM	1.4
G6P	1.3 ± 0.4 (5)[b]	0.66	1.4 ± 0.4 (5)	1.0
F6P	0.5 ± 0.2 (5)[b]	0.01	0.5 ± 0.2 (5)	0.02
FBP	0.38(2)[b]	0.14	0.23 (2)	0.52
DHAP	0.93 ± 0.07	2.0	0.54	3.6
G3P	ND	0.08	NM	0.14
1,3BPG	ND	0.0009	NM	0.001
3PG	ND	0.006	NM	0.009
2PG	ND	0.003	NM	0.004
PEP	0.32	0.0002	NM	0.0003
Pyr	8.5 ± 3.6	2.5	4.2 (2)	2.6
lactate	33	Fixed	NM	Fixed
F2,6BP ($\times 10^{-3}$)	4.2 ± 0.8 (3)[b]	Fixed	NM	Fixed
citrate	NM	Fixed	NM	Fixed
ATP	8.7 ± 3 (5)[b]	8.4	7.9 ± 4 (5)	7.7
ADP	2.7 ± 1.3	2.2	1.8 (2)	2.1
AMP	0.4 (2)[b]	1.3	NM	1.2
Pi	7.5 (2)[b]	Fixed	7.8 (2)[b]	Fixed
NADH	NM	0.005	NM	0.005
NAD^+	NM	1.34	NM	1.34
Glycolytic flux	16 ± 12 (5)[b]	20	21 ± 9 (5)[b]	29

Metabolite concentrations in mM; flux in nmol lactate min^{-1} (mg cellular protein)$^{-1}$. Values taken from [a][10]. [b]Present study. [c]For this condition, HK and HPI activities were determined in cells exposed to hypoxia by 24 h; GLUT activity was estimated from the protein content obtained by Western-blot analysis (Fig. 2); the ATPase rate was also adjusted to a value of 4.5×10^{-3}. Figures in parentheses indicate number of independent cellular batches assayed. NM, not measured; ND, not detected. The fixed values used for modeling were those experimentally determined in cells, except for Pi which was adjusted to the free concentration.

with Vm_r as the maximal rate in the reverse (gluconeogenic) direction.

The kinetics for TPI, PGAM and ENO were depicted by mono-substrate simple reversible Michaelis–Menten equation:

$$v = \frac{Vmf\frac{[S]}{Ks} - Vmr\frac{[P]}{Kp}}{1 + \frac{[S]}{Ks} + \frac{[P]}{Kp}}$$

in which [S] and [P] are the respective concentrations of substrates and products with their respective affinity constants.

PFK-1 is an allosteric enzyme showing cooperative behavior with respect to F6P and hyperbolic kinetics with respect to ATP. The rate equation for this tetrameric enzyme was the concerted transition model of Monod, Wyman and Changeux for exclusive ligand binding (F6P, activators, and inhibitors) [25] together with mixed-type activation (F2,6BP or AMP or Pi) and simple Michaelis–Menten terms for ATP and reverse reaction. ATP (at high concentrations) and citrate are the allosteric inhibitors. L is the allosteric transition constant; Ka_{F26BP} is the activation constant for F26BP; Ki_{CIT} and Ki_{ATP} are the inhibition constants for citrate and ATP; α and β are the factors by which K_{F6P} and Vm change when an activator is bound to the active enzyme form (R conformation in the Monod model).

$$v = Vm\left(\left(\frac{\frac{[ATP]}{K_{ATP}}}{1+\frac{[ATP]}{K_{ATP}}}\right)\left(\frac{1+\frac{\beta F26BP}{\alpha Ka_{F26BP}}}{1+\frac{F26BP}{\alpha Ka_{F26BP}}}\right)\left(\frac{\frac{F6P\left(1+\frac{F26BP}{\alpha Ka_{F26BP}}\right)}{K_{F6P}\left(1+\frac{F26BP}{Ka_{F26BP}}\right)}\left[1+\frac{F6P\left(1+\frac{F26BP}{\alpha Ka_{F26BP}}\right)}{K_{F6P}\left(1+\frac{F26BP}{Ka_{F26BP}}\right)}\right]^3}{\frac{L\left(1+\frac{[CIT]}{Ki_{CIT}}\right)^4\left(1+\frac{[ATP]}{Ki_{ATP}}\right)^4}{\left(1+\frac{F26BP}{Ka_{F26BP}}\right)^4}+\left[1+\frac{F6P\left(1+\frac{F26BP}{\alpha Ka_{F26BP}}\right)}{K_{F6P}\left(1+\frac{F26BP}{Ka_{F26BP}}\right)}\right]^4}\right)-\left(\frac{\frac{[ADP][FBP]}{K_{ADP}K_{FBP}Keq}}{\frac{[ADP]}{K_{ADP}}+\frac{[FBP]}{K_{FBP}}+\frac{[ADP][FBP]}{K_{ADP}K_{FBP}}+1}\right)\right).$$

The ALDO rate equation was the reversible Uni–Bi Michaelis–Menten equation.

$$v = \frac{Vmf\frac{[FBP]}{K_{FBP}} - Vmr\frac{[DHAP][G3P]}{K_{DHAP}K_{G3P}}}{1 + \frac{[FBP]}{K_{FBP}} + \frac{[DHAP]}{K_{DHAP}} + \frac{[G3P]}{K_{G3P}} + \frac{[DHAP][G3P]}{K_{DHAP}K_{G3P}}}$$

The GAPDH kinetics was described by a simplified ordered Ter–Bi reversible Michaelis–Menten equation:

$$v = \frac{Vmf\frac{[NAD][G3P][Pi]}{K_{NAD}K_{G3P}K_{Pi}} - Vmr\frac{[BPG][NADH]}{K_{BPG}K_{NADH}}}{1 + \frac{[NAD]}{K_{NAD}} + \frac{[NAD][G3P]}{K_{NAD}K_{G3P}} + \frac{[NAD][G3P][Pi]}{K_{NAD}K_{G3P}K_{Pi}} + \frac{[BPG][NADH]}{K_{DPG}K_{NADH}} + \frac{[NADH]}{K_{NADH}}}.$$

Rate equations for PGK and LDH were represented by the random Bi–Bi reversible Michaelis–Menten equation for non-interacting substrates (α and β = 1).

$$v = \frac{Vmf\frac{[A][B]}{\alpha KaKb} - Vmr\frac{[P][Q]}{\beta KpKq}}{1 + \frac{[A]}{Ka} + \frac{[B]}{Kb} + \frac{[A][B]}{\alpha KaKb} + \frac{[P][Q]}{\beta KpKq} + \frac{[P]}{Kp} + \frac{[Q]}{Kq}}.$$

PYK kinetics was represented by the concerted transition model of Monod, Wyman and Changeux rate equation for exclusive ligand binding including PEP as well as FBP activation and ATP inhibition, with simple Michaelis–Menten terms for ADP and reverse reaction.

$$v = Vm\left(\left(\frac{\frac{[ADP]}{K_{ADP}}}{1+\frac{[ADP]}{K_{ADP}}}\right)\left(\frac{\frac{PEP}{K_{PEP}}\left[1+\frac{PEP}{K_{PEP}}\right]^3}{\frac{L\left(1+\frac{[ATP]}{Ki_{ATP}}\right)^4}{\left(1+\frac{FBP}{Ka_{FBP}}\right)^4}+\left[1+\frac{PEP}{K_{PEP}}\right]^4}\right)-\left(\frac{\frac{[ATP][PYR]}{K_{ATP}K_{PYR}Keq}}{\frac{[ATP]}{K_{ATP}}+\frac{[PYR]}{K_{PYR}}+\frac{[ATP][PYR]}{K_{ATP}K_{PYR}}+1}\right)\right).$$

The ATPases rate defined as the ATP-consuming cellular processes was depicted as mass-action irreversible reaction, in which k was the rate constant and Si was the substrate concentration.

$$v = k\prod_i Si.$$

The DHases and AK were included as reversible mass-action reactions, in which k_1 and k_2 are the rate constants, Si is the concentration of substrate and Pj is the concentration of product.

$$v = k1\prod_i Si - k2\prod_j Pj$$

The rest of glycolytic branches were adjusted to irreversible constant flux.

3. Results and discussion

3.1. Glycolytic enzyme activities, intermediary concentrations and fluxes in tumor cells

A recurrent difficulty encountered in building kinetic models of metabolic pathways is the lack of all the required kinetic data of the pathway under study, evaluated in the same cellular model, and determined under the same experimental conditions. Despite these inconveniences, some models have been reported for glycolysis in erythrocytes [26,27], yeast [28] and the human-infecting parasites *Trypanosoma brucei* [29] and *Entamoeba histolytica* [16].

Although there is sufficient kinetic information on glycolytic enzymes from a wide variety of tumor cells, most studies are not

usually accompanied by thorough cellular metabolic characterizations reporting metabolite concentrations and metabolic fluxes. This is particularly evident in studies based only on determinations of transcriptional changes, from which hypotheses and explanations are formulated about changes in metabolic fluxes and cellular function [reviewed and discussed in 9]. Hence, in order to have a complete kinetic characterization of the glycolytic pathway and its branches in the tumor cells studied here, the maximal velocities in the forward (Vm_f) and reverse (Vm_r) reactions and *Km* values for substrates (Km_s), products (Km_p) and effectors for each glycolytic enzyme were determined in cytosolic extracts from AS-30D and HeLa cells at 37 °C and pH 7.0 (Table 1). A pH value of 7.0 was chosen because the intracellular pH varies from 7.2 to 6.8 when cells are actively consuming glucose [30]. Due to thermodynamic constraints, HK, PFK-1 and PYK activities were only determined for the forward reaction.

In general, most of the enzyme activity (*i.e.*, *Vm*) values (Table 1) were in agreement with those previously reported for the same tumor cell lines [31,32]. In tumor cells, approximately 50–70% of HK activity is bound to mitochondria [10,33,34]; thus, to have an accurate determination of the total HK activity, detergent-permeabilized cells were used (Table S3). Remarkably, HK, PFK-1 and PGAM activities found in cytosolic extracts were 7.6, 3.5 and 14 times higher in AS-30D than in HeLa cells; which contrasted with the similar values obtained for the rest of the pathway enzymes in both cells (Table 1). HK and PFK-1 are 153 and 27 times lower in rat normal hepatocytes (3 and 10 mU/mg protein, respectively) than in the AS-30D hepatocarcinoma [10]. On the other hand, HK activity in human muscle cells is 10 times lower whereas PFK-1 activity in human brain is 3 times higher than in HeLa cells (6 and 258 mU/mg protein, respectively) [35,36]; however, for a more rigorous comparison with HeLa cells, normal proliferating cervix epithelial cells from which these tumor cells derived, should be used.

The *Km* values were similar in the two cell types (Table 1) and were within the same interval found in the BRENDA database (http://www.brenda-enzymes.info/) determined for normal and tumor cells.

The previously reported value for the glycolytic flux in AS-30D cells under normoxia and 5 mM glucose was 21 nmol min^{-1} (mg cellular protein)$^{-1}$ [10] which was used as reference in the present study (Table 3). On the other hand, in HeLa cells a value of 16 ± 12 nmol min^{-1} (mg cellular protein)$^{-1}$ (n = 5) under normoxic conditions was obtained in the present study (Table 4), which was lower than the previously reported value of 32 ± 10 nmol min^{-1} (mg cellular protein)$^{-1}$ [10], indicating variability within the same cell line from culture passage to culture passage. For comparison, normal rat hepatocytes and normal Chinese hamster ovary cells (CHO-K1) show glycolytic flux values of 2.4 and 8 nmol min^{-1} (mg cell protein)$^{-1}$, respectively [10,37]. Thus, the tumor cells used here indeed exhibit increased glycolysis rates compared to normal cells. Glycolytic metabolite concentrations were also previously reported for AS-30D cells incubated with 5 mM glucose [10] and used as reference (Table 3), whereas for HeLa cells under normoxia, values for some metabolites were re-determined (Table 4), finding no statistical difference with those previously reported [10].

The enzyme activities, fluxes and intermediary concentrations of the main glycolytic branches were also evaluated (Table 2): glycogen synthesis and degradation, PPP, triglyceride and serine synthesis, and MPM.

Regarding glycogen, HeLa cells showed 5.2 fold higher content than AS-30D cells and 2.3 fold increased PGM activity (Table 2). The glucose-1-phosphate (G1P) intracellular concentration (0.08 mM; Table 2) was lower than its glycolytic precursor G6P in AS-30D cells (5.3 mM; Table 3). Under the steady-state conditions used, in which extracellular glucose concentration is 5 mM (see Experimental procedures section), the glycogen synthesis and degradation rates were 10–18 times lower (Table 2) than the glycolytic fluxes (Tables 3 and 4) in both tumor cells; with the exception of the glycogen degradation flux in HeLa cells which was 75% the glycolytic flux. The most probable reason for the higher activity in the glycogen degradation branch in HeLa cells was that these are cultured in Dulbecco-MEM medium containing 25 mM glucose, whereas the glucose concentration found in AS-30D ascites fluid is 0.026 mM [38]. Cultivation of HeLa cells under high (25 mM) glucose induces the expression of the low affinity glucose transporter GLUT1, whereas AS-30D hepatoma developed intra-peritoneally in rats predominantly express the high affinity GLUT3 [24]. In consequence, the incubation of HeLa cells in fluxes assay medium containing lower glucose (compared to culture medium) most probably promoted strong activation of glycogen degradation to compensate for the diminished glucose uptake; this compensatory mechanism was apparently not required in AS-30D hepatoma.

In the oxidative section of PPP (Table 2), higher G6PDH activity was found in HeLa than in AS-30D cells, but similar 6PG concentrations. On the other hand, the activities of the PPP non-oxidative section enzymes TA and TK were similar to reported values for the same and other tumor cells (0.019–0.208 and 0.022–0.108 U (mg protein)$^{-1}$, respectively) [17,39]. A lower Ery4P concentration in comparison to that of glycolytic intermediaries (G6P, FBP, and DHAP) was determined, which was slightly higher than the previously reported value for Krebs ascites hepatoma cells (0.5 nmol/mg cellular protein) [40]. The lower PPP flux and enzyme activities (Table 2) compared to glycolytic flux (see text above for values) and enzyme activities (Table 1) suggested low nucleotide synthesis and hence negligible cellular proliferation, as expected from incubations made in a saline buffer for short times (3–10 min). For A549 lung carcinoma and C6 rat glioma, PPP fluxes of 1 and 6 nmol/min*mg protein, respectively, were determined by using radio-labelled glucose and lengthy incubations of 4–6 h in culture medium with glucose and fetal bovine serum, conditions under which cellular growth is favored [41,42]. Then, it seems possible that the PPP fluxes, determined here from 6PG changes (Table 2), were underestimated as the variation in the cellular 6PG content was small and close to the lower detection limit of the method used. Further evaluation of the PPP flux in AS-30D and HeLa cells either with radio-labelled glucose or under cell growth conditions for longer times should resolve this apparent discrepancy.

Low or negligible αGPDH activities, which are involved in triglyceride synthesis, have been reported for several tumor cells [43]; accordingly, αGPDH activity was not detected in AS-30D and HeLa cells [10]. Triglyceride synthesis can also be initiated by DHAP acylation in a reaction catalyzed by DHAP-acyltransferase [44]; however, this enzyme was not determined in the present study and this branch was not included in the model.

A previous report indicated that serine metabolism is accelerated in tumor cells [45]; however, the activity of 3-phosphoglycerate dehydrogenase was not detected when measured in the 3PG oxidation direction (Table 2) and thus, this branch was not included in the model. Alanine transaminase activity (AlaTA) measured in the pyruvate synthesis direction was low in both AS-30D and HeLa cells (Table 2). These low activities correlated with undetectable alanine levels in cellular extracts.

The MPM rate was 11.7 fold lower than the lactate production rate, suggesting that anaerobic glycolysis was favored. It might be possible that the mitochondrial pyruvate transporter expressed in AS-30D cells also has low affinity and low rate as described for Morris 44 and 3924A hepatomas (Vm = 5–12 mU/mg mitochondrial protein and Km_{Pyr} = 0.74–1.1 mM) [46]. The expression of a low activity/low affinity pyruvate transporter would favor a higher pyruvate flux towards lactate because of LDH higher activity and affinity (Vm = 2.0 U/mg cellular protein, Table S3; Km_{Pyr} = 0.13 mM, Table 1). Contributing to the unusually high endogenous pyruvate pool (Tables 3 and 4) may be the active oxidation of alternative substrates such as glutamine, glutamate and proline, which generate malate and hence pyruvate by the action of over-expressed malic enzyme in cancer cells [38,47]. In addition, the onset of the Crabtree effect (OxPhos inhibition by external glucose) should also promote an elevation in the intracellular pyruvate pool [30].

3.2. Building and refinement of the kinetic model of AS-30D glycolysis

The kinetic model of glycolysis in AS-30D cells was constructed by using the Gepasi software. The kinetic parameters *Vm*, *Km* for substrates, products and modulators for the pathway enzymes and glucose transporter from external glucose to lactate production as well as the enzyme activities and fluxes of the pathway branches experimentally determined were used to fulfill the parameters of the rate-equations describing each reaction as detailed in the Experimental procedures section. The metabolite concentrations and the pathway fluxes of glycolysis determined *in vivo* under steady-state conditions (Table 3) and the control distribution obtained by elasticity analysis previously reported by our research group [10] (Table 5) were used as reference parameters for model validation.

In consequence, for model building and validation, a refinement process was recurrently necessary, which in turn prompted an experimental re-evaluation of the kinetic properties of some enzymes as well as the determination of neglected metabolite concentrations and the inclusion of some branches to improve model reproduction of *in vivo* pathway behavior. Thus, this dynamic interplay between modeling and experimentation led to several model and rate equation modifications, from which the three most important are described below.

3.2.1. Kinetics of PFK-1

The first draft of the model included the reactions from external glucose to lactate production and the branch of glycogen metabolism (Fig. 1), in which a simplified version of the PFK-1 rate-equation (hyperbolic kinetics) was used. However, G6P level was too high whereas those of DHAP and G3P were too low. Thus, an improvement of the PFK-1 reaction was necessary.

There is a lack of detailed kinetic analyses of PFK-1 in normal and tumor cells, in which a simple Hill equation for only one modulator is used. Hence, a kinetic characterization of PFK-1 was carried out in AS-30D and HeLa cells (see Experimental procedures section), resulting in a rate-equation that followed the concerted transition model of Monod, Wyman and Changeux together with non-essential activation by F2,6BP (or any other allosteric activator) (Moreno-Sánchez R., Marín-Hernández A., Encalada R. and Saavedra E., unpublished results). The intracellular concentrations of F2,6BP, AMP, ATP and citrate were also determined (Tables 3 and 4). As the activating effect of F2,6BP overcame the inhibitory effect of citrate and ATP, at the tumor physiological concentrations of these modulators (see a simulation in Fig. S1 in supplementary material), the PFK-1 rate in the presence of physiological F2,6BP was 2 fold higher with the concomitant increased in FBP and DHAP to near-physiological levels. However, a marked decrease in the Glu_{in}, G6P and F6P concentrations was attained.

3.2.2. Kinetics of HPI

Through modeling it was noted that a decrease in the HPI activity resulted in a better prediction of the G6P concentration and the glycolytic flux. Hence, the effect of a wide variety of metabolites (ATP, AMP, Pi, PPi, citrate, Ery4P, DHAP, G1P, lactate, 6PG, FBP and F2,6BP) on HPI activity was examined. Most of them showed no effect (Table S5 in supplementary material); in contrast low *Ki* values for Ery4P (0.8–2.5 μM), 6PG (6.8–18 μM) and FBP (60–170 μM) were determined (Table S6). Thus, multiple competitive-type inhibition by Ery4P (Fig. S2), 6PG and FBP was incorporated in the HPI rate-equation. The potent HPI inhibition by these metabolites was not particular of the tumor enzyme, since it was previously reported for the normal rat brain, and rabbit liver and muscle HPIs [48–50] and they also modulated the enzymes from rat hepatocytes, yeast and *E. histolytica* (Table S6). Therefore, the intracellular concentrations of 6PG and Ery4P were also determined in the tumor cells, and in consequence the oxidative section of PPP and TK reaction with their corresponding fluxes (Table 2) and metabolite interactions with HPI were also included in the model (Fig. 1).

3.2.3. Kinetics of the FBP consuming block of enzymes and GAPDH

By including the two modifications described above, the modeled FBP concentration was still several times lower than the physiological concentration, indicating an unrealistic high rate by the consuming block of this metabolite. Thus, the effects of G6P, F6P, Pi, ATP, AMP, Ery4P, F2,6BP and PPi on the enzymes of the ALDO–ENO segment were tested (see Table S5).

ALDO activity was not modulated by any of these metabolites. Although GAPDH was inhibited by ATP (with non-competitive inhibition, $Ki = 4.3$ mM) and ENO was inhibited by DHAP and ATP (non-competitive inhibition, $Ki = 31$ mM, and uncompetitive inhibition, $Ki = 14$ mM, respectively), these *Ki* values were far from the physiological concentrations, and their effects were not included in the rate-equations.

GAPDH from AS-30D cells showed low affinity for Pi (Table 1; Fig. S3) which suggested that Pi availability might regulate the enzyme activity. High Km_{Pi} values for GAPDH from bovine liver, human muscle and sarcoma [51,52] have also been documented. Thus, contrary to other glycolysis kinetic models in which Pi is considered saturating and hence it is not included as pathway metabolite, in the present model Pi was included in the GAPDH rate-equation. On the other hand, from the total intracellular Pi concentration determined (Table 3) only 53% [22] was assumed to be free (*i.e.*, 2.5 mM); this free Pi concentration was used for modeling and was in agreement with values previously determined by nuclear magnetic resonance in rat liver and heart (1.3–2.8 mM) [53,54].

3.2.4. Properties of the kinetic model of glycolysis in AS-30D hepatoma cells

By incorporating (i) the PFK-1 complex rate equation, (ii) the inhibition of FBP, 6PG and Ery4P on HPI, and (iii) Pi in the GAPDH rate-equation, the kinetic model was able to predict with high accuracy the concentration of most of the pathway metabolites and flux rate determined in living cells (Table 3). The most significant exceptions were the predicted FBP (4.8 times lower) and F6P (50 times lower) concentrations. It was found that the FBP steady state concentration directly depended on the Pi concentration within the reported physiological range (Table S7). On the other hand, only by decreasing to 20% the PFK-1 activity, the F6P reached the physiological level; however, this decrease was not experimentally supported because of the strong activation by F2,6BP, AMP and/or Pi. Moreover, under this last condition of 20% activity, PFK-1 became the main flux control step, which was in disagreement with the results obtained by elasticity analysis [10]. Hence, still another unknown kinetic mechanism seems to also modulate the *in vivo* PFK-1 rate.

3.2.5. Control distribution of glycolysis in AS-30D

The analysis performed by Gepasi provided the C^J_{Ei} of all the pathway steps (Table 5). Modeling indicated that the first three reactions of glycolysis exerted most of the flux-control with HK ≥ HPI > GLUT ($\Sigma C^J_{Ei} = 1.04$; Table 5). This control distribution was in agreement with the C^J_{Ei} obtained by elasticity analysis, which indicated that the G6P producer block (GLUT and HK) exerted the main flux-control ($\Sigma C^J_{Ei} = 0.65$–0.71) [10], whereas the C^J_{HPI} value was not possible to be discerned in the previous study, because the high experimental dispersion masked flux-control differences among the different blocks of enzymes analyzed.

HK and HPI showed high flux-control because they were strongly inhibited by glycolytic and PPP intermediaries. It was previously demonstrated [10] that HK exerted significant control on flux in cancer cells because it was strongly inhibited by its product G6P, despite its higher levels of expression compared to normal cells. In particular, AS-30D cells over-expressed the HK-II isoform [24] which partitioned between the cytosol and mitochondria, the latter showing the same affinity constants for glucose, ATP and G6P than the former, cytosolic HK II [10]. Thus, although a hallmark of tumor cells is the

Table 5
Flux control coefficients obtained *in vivo* (cells) and by kinetic modeling.

Enzyme	C^J_{Ei}				
	AS-30D	AS-30D model		HeLa model	
	In vivo[a]	5 mM Glucose	1 mM Glucose	Normoxia	Hypoxia
GLUT +		0.2	0.12	0.39	0.32
HK	0.71[a]	0.44	0.50	0.08	0.2
HPI +	−0.02[a]	0.4	0.46	0.05	0.1
PPP +		−0.004	−0.009	−0.009	−0.005
glycogen synthesis		−0.1	−0.1	−0.1	−0.06
Glycogen degradation	NM	0.05	0.11	0.57	0.33
PFK-1	0.06[a]	0.02	0.03	0.03	0.12
ALDO + TPI + GAPDH + PGK + PGAM + ENO + PYK + LDH	0.24[a]	0.08 (GAPDH 0.05)	0.009	0.01	0.06
MPM	NM	0.003	0.02	−0.004	−0.001
TK	NM	0.01	0.023	0.014	0.01
ATPases	NM	−0.1	−0.16	−0.02	−0.05

[a] Values taken from [10]. PPP, pentose phosphate pathway; MPM, mitochondrial pyruvate metabolism. NM, not measured. For AS-30D, both conditions were modeled under normoxia. For HeLa, both conditions were modeled in the presence of 5 mM glucose.

increased activity of the glycolytic enzymes, the same enzyme activity regulatory mechanisms are apparently preserved to avoiding unrestricted increase in flux, which in turn can lead to cell death because of the turbo design of glycolysis [55]. On the other hand, HK also exerts significant flux control in normal cells [26,56] making this step less suitable for specific drug targeting in cancer cells.

In turn, HPI displayed a high C^J_E, despite being one of the most active enzymes in the pathway when determined under *Vm* conditions in the absence of modulators (Table 1). However, the potent combined HPI inhibition by FBP and the PPP intermediaries 6PG and Ery4P led to severe activity decrease, becoming now limiting for pathway flux. The modulation of HPI activity by these metabolites might be a control mechanism of the G6P concentration which in turn may exert control on (a) the synthesis of glycogen; (b) the PPP flux for NADPH and ribose-5P syntheses; (c) the production of UDP-glucuronate for proteo-glycan and glycoproteins synthesis and xenobiotic detoxification; and (d) the cellular ATP homeostasis by avoiding its depletion through an enhanced HK reaction. Remarkably, this HPI inhibition was also present in the yeast and ameba enzymes. As the potent inhibition on HPI here described was not considered in previous published models of glycolysis, which might change the control distribution, the putative HPI controlling role remains to be experimentally evaluated in other biological systems. On the other hand, the significant HPI flux control in AS-30D cancer cells (*cf.* Table 5), and its negligible controlling role in normal cells [26,56], indicates that this step is a suitable therapeutic target.

The results on HPI and GAPDH kinetics emphasize the importance, for metabolic modeling, of an extensive knowledge of the enzyme kinetic properties, which should not be restricted to the sole characterization with their substrates, but also to its interaction with its products and with other pathway intermediaries, which are not always assayed when studying the purified enzymes. This has been previously demonstrated by reconstitution of pathway segments of amebal glycolysis [57], in which interactions with non-substrate metabolites but pathway glycolytic intermediaries were elucidated for several enzymes.

GLUT displayed significant flux control ($C^J_{GLUT} = 0.2$; Table 5) as previously suggested by elasticity analysis [10] and its kinetic properties [24]. From the main four isoforms (GLUT1–4), AS-30D cells mainly express GLUT3 which has a high affinity for glucose ($Km = 0.52$ mM) [24]. Moreover, by over-expressing all GLUT isoforms in *Xenopus* oocytes and determining the kinetics parameters with 2-deoxyglucose, it was previously concluded that GLUT3 is the transporter with the highest catalytic efficiency [reviewed in 5]. In AS-30D cells, GLUT displayed lower activity and catalytic efficiency (*Vm*/*Km*) than HK and HPI; however, the inhibitory effect on the latter two by glycolytic and PPP metabolites decreased their activities to levels that conferred flux-controlling roles. In contrast, in the kinetic models of glycolysis in yeast [28], *T. brucei* [29], *E. histolytica* [16] and heart [56], GLUT contributed by >50% to flux-control. This difference in GLUT flux control between tumor cells and heart indicates that this step might not be an adequate target for cancer treatment, because its inhibition would preferentially affect normal cells over tumor cells.

The rest of the flux-control (0.08) was found in the ALDO–LDH segment (Table 5), which was also in agreement with that obtained by elasticity analysis ($\Sigma C^J_{Ei} = 0.24$) [10]. Within this segment, most of the control was accounted by GAPDH ($C^J_{GAPDH} = 0.05$), due to its Pi low affinity and hence its dependence on the variation of the Pi concentration in AS-30D cells (Table S7). The ATP demand (ATPases) showed a low flux control but of the negative sign, indicating that this reaction competes with the glycolytic ATP-consuming steps for ATP thus inhibiting the glycolytic flux.

3.2.6. Why a step controls flux?

The HK elasticity coefficient (Table S8) and the catalytic efficiency for ATP (*Vm*/*Km*) were among the lowest in both AS-30D and HeLa glycolysis, indicating near-saturation with concomitant activity insensitivity to variations in ATP, relatively lower transformation efficiency and hence flux limitation at this level. In turn, the reasons for the HPI high flux control coefficient resided in its step-wise increasing elasticities (sensitivities) towards the potent inhibitors FBP, 6PG and Ery4P, and low elasticity for its product F6P, indicating saturation, and hence strong inhibition and prevalence of the reverse over the forward reaction. Similarly, GLUT catalytic efficiency was the lowest among the pathway steps, indicating strong flux restriction; in addition, in HeLa cells, GLUT elasticity for its product, Glu_{in}, was one of the lowest, indicating near-saturation and perhaps product-inhibition and significant reaction reversibility and correlating with a higher GLUT flux control in these cells. On the other hand, the low flux-control exerted by PFK-1 is explained by the low elasticity towards activators, indicating saturation and hence full activation. If PFK-1 were not fully activated, it would very likely the main controlling step as its elasticity towards F6P is the lowest. On the other hand, the PFK-1 elasticities for citrate, and for their products FBP and ADP, were extremely low because these metabolites were not sensed due to the high *Ki* and *Km*, and low intracellular levels.

3.2.7. Control of metabolite concentrations

The control of the concentration of G6P, PEP and ATP depended on GLUT, HK, HPI and ATPase activities in AS-30D glycolysis and on GLUT, glycogen degradation and ATPase in HeLa glycolysis (Table S9). For the F6P concentration, PFK-1 in both AS-30D and HeLa glycolysis was the predominant controlling step, as expected.

3.2.8. Model robustness

The modeled pathway behavior (*i.e.*, flux-control and concentration control distribution, flux rates and metabolite concentrations) was not significantly altered by changing (decreasing by half or increasing by 2 times) the kinetic parameters of most steps and PPP flux (data not shown). Exceptions were (i) control distribution and/or metabolite concentrations, which varied by more than 50% when changing the main controlling steps GLUT, HK, HPI, PFK-1 and GAPDH *Vm* values (AS-30D model) or GLUT, glycogen degradation, PFK-1 and GAPDH *Vm* values (HeLa model, see below); (ii) FBP concentration, which varied by 21–100% when changing ALDO *Vm* and *Km* values in both models; and (iii) DHAP concentration, which varied by 9–100% when changing TPI, GAPDH, PGK, PGAM, ENO and PYK *Km* values (AS-30D) or only TPI *Km* values (HeLa). Both models were also highly sensitive to changes in the ATPase kinetics, revealing that this step is the weakest component in conferring stability to the pathway.

Notwithstanding the enlisted exceptions, the predicted pathway behavior showed satisfactory robustness, further validating the models constructed for both cancer cell lines.

3.3. Kinetic model of glycolysis in HeLa tumor cells

The kinetic model for HeLa cells glycolysis was constructed based also on the experimental parameters determined in these cells regarding enzyme activities (Table 1), metabolite concentrations and fluxes of the glycolytic pathway (Table 4) and its branches (Table 2), and the rate equations used in the AS-30D model.

The majority of the metabolite concentrations and fluxes predicted by the model correlated well with the *in vivo* concentrations except for F6P and PEP, which were 50- and 1600-times lower, respectively (Table 4). These discrepancies indicated that some kinetic experimentation-based refinement was still needed, most probably at the level of PFK-1 and ALDO, and PYK.

According to the model, the main flux controlling steps in HeLa cells, grown under normoxic and high glucose (25 mM) conditions, and assayed in the presence of physiological glucose (5 mM), were the glycogen degradation pathway and GLUT ($C^J_{glycogen\ degradation} + C^J_{GLUT} = 0.96$), whereas the control exerted by the block of HK + HPI + PFK-1 was 0.16 (Table 5). The higher control attained by GLUT in HeLa cells compared to AS-30D was caused by the over-expression of the GLUT1 isoform, which displays low rate in these cells (0.017 nmol/min* mg cellular protein) and low affinity for glucose (9 mM), resulting in a lower catalytic efficiency than that of GLUT3 in AS-30D cells [24]. At physiological glucose concentration (5 mM), the rate equation for GLUT1 predicts an activity of 25% of its maximal activity (4 nmol min^{-1} mg cellular $protein^{-1}$), which cannot completely account for the observed glycolytic flux (16 ± 12 nmol lactate min^{-1} mg cellular $protein^{-1}$). In consequence, the glycogen degradation pathway activates to provide the bulk of glucose equivalents to reach the observed high glycolytic flux.

The high flux through the glycogen degradation pathway and the higher PGM activity determined in HeLa cells, compared to AS-30D cells, supported a relevant role for this pathway in delivering glucose equivalents for glycolytic flux (Table 2). In fact, HeLa cells incubated in the absence of glucose were able to produce lactate (7 nmol·min^{-1}·mg cellular $protein^{-1}$), which corresponded to 22% of the lactate produced in its presence. In contrast, lactate production in AS-30D cells was completely dependent on available external glucose [10]. On the other hand, at 25 mM glucose, the predicted GLUT1 rate in HeLa cells (11.7 nmol min^{-1} mg cellular $protein^{-1}$) can easily cope with the required glucose supply for the glycolytic pathway, which brings about a decreased flux control exerted by both glycogen degradation and GLUT (data not shown). Moreover, it is well documented that glycogen phosphorylase is inhibited by high glucose and G6P levels, with the consequent decrease in glycogenolytic flux [58]. It might be possible that when HeLa cells are incubated with 5 mM glucose, the intracellular concentrations of these metabolites concomitantly also diminish as a consequence of the low GLUT activity, thus favoring glycogen phosphorylase activation, increasing glycogenolysis and hence acquiring higher flux-control.

Thus, the different control distribution between AS-30D and HeLa cells was probably related to the environmental prevailing conditions in which cells were grown. The low glucose concentration encountered by AS-30D cells in the rat intraperitoneal cavity (0.026 mM) favored the expression of a high affinity GLUT and led to a relatively low glycogen content, whereas the HeLa cell high-glucose containing culture medium (25 mM) favored the expression of a low affinity GLUT and led to high glycogen content.

3.4. Kinetic modeling under different steady-states

It is worth emphasizing that the control distribution as obtained by modeling can only be applied to the specific steady-state condition analyzed, which depended on a particular set of enzyme activities expressed in the cells. Therefore, it was interesting to test the validity of the model predictions in cells subjected to other environmental conditions.

During tumor growth, cells localized far from blood vessels are exposed to hypoxia and nutrient starvation. It is well known that under hypoxia the transcription factor HIF-1α induces an increase in the transcription of most glycolytic genes resulting in an over-expression of the enzymes and transporters of this pathway [reviewed in 5]. On the other hand, under low glucose concentration, an increase transcription of HK-II, PFKB3, GLUT1 and GLUT3 induced by AMP kinase has been observed [59,60].

With the validated kinetic models, low availability of external glucose (for AS-30D) and hypoxia (for HeLa) conditions were examined. To this end, it seemed that only a small set of data was needed to be experimentally re-evaluated by focusing on the steps with the highest control. Although a generalized increased activity under hypoxia in the glycolytic enzymes has been documented for most tumor cells [reviewed in 1], a higher increase activity in non-controlling steps does not affect pathway flux rate and flux-control distribution (Section 3.2.8 above).

3.4.1. Modeling AS-30D glycolysis under low glucose concentration

Steady-state intermediary concentrations and glycolytic flux determined in AS-30D cells incubated with 1 mM glucose were ~50% lower for G6P, F6P, G3P and Pyr, and flux rate, and one order of magnitude lower for FBP and DHAP (Table 3). The AS-30D kinetic model predicted well the values for flux and G6P, FBP, G3P and Pyr concentrations found in the cells, but for DHAP and G3P the values were 4 times higher and 4.2 times lower, respectively (Table 3). Essentially the same flux-control distribution was attained under low glucose (HK ≥ HPI > GLUT), with the glycogen degradation branch gained more control, as expected (Table 5).

3.4.2. Modeling HeLa glycolysis under hypoxic conditions

HeLa cells exposed to hypoxia did not show significant changes in G6P, F6P and ATP steady-state concentrations, whereas a 31% increased glycolytic flux was indeed found compared to cells grown under normoxia (Table 4). Increased enzyme activities under hypoxia for HK and HPI were also determined (37% and 30%, respectively) whereas a 252% increased protein content for GLUT was determined by Western-blot analysis (Fig. 2) and then a corresponding increase in transport activity was assumed for modeling. By introducing these new parameters, the kinetic model satisfactorily predicted the flux rate and the metabolite concentrations (Table 4). In addition, hypoxia did not bring about a change in the control distribution (glycogen degradation > GLUT > HK), although the difference in the control exerted by glycogen degradation and GLUT compared to normoxia (31%) was mainly transferred to HK, PFK-1 and the final pathway segment (Table 5).

The experiment of subjecting HeLa cells to hypoxia and nutrient starvation and determining fluxes, activities and metabolite concentrations is difficult to achieve because of low cell number yields. Therefore, the HeLa model was used to predict the pathway behavior under both conditions (hypoxia and 1 mM glucose; data not shown). The results showed a similar control distribution to that obtained under normoxia and 5 mM glucose (column 5 of Table 5) although with decreases in flux and metabolite concentrations by 36–86%, compared to hypoxia alone (column 6 of Table 5). These accurate predictions under a variety of physiological steady-state conditions revealed again high robustness of the kinetic models adding further validation.

3.5. Enzyme titration for the identification of the best drug targets

The kinetic models allow the relationship between glycolytic flux and a given enzyme activity to be analyzed (Fig. 3). As long as the

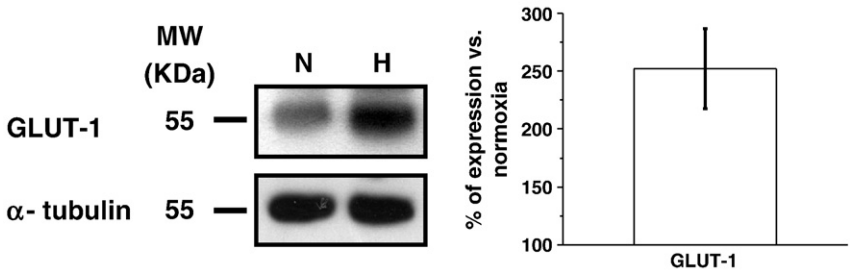

Fig. 2. Glucose transporter protein content after hypoxia treatment in HeLa cells.Bar data represent the mean ± SD of at least three different preparations. N, normoxia; H, hypoxia. Western-blot analysis was carried out according to reference [19].

models may reproduce the *in vivo* pathway behavior, they are a valid tool for identifying the drug targets with the highest therapeutic potential in a metabolic pathway. Thus, GLUT, HK, HPI, PFK-1, TPI and PYK activities were varied in the AS-30D hepatoma glycolysis model, or GLUT, HK, HPI, TPI and the glycogen degradation branch in the HeLa model, to establish how much these potential drug targets should be inhibited for attaining significant decrement in the glycolytic flux and ATP concentration. To decrease the pathway flux (or the ATP concentration; data not shown) by 50%, it was required to inhibit, individually, the main controlling steps HK, HPI or GLUT by 76–78% in AS-30D glycolysis (Fig. 3A), whereas those of HeLa glycolysis GLUT, HK, HPI or glycogen degradation required 87–99% inhibition (Fig. 3B). In contrast, to achieve a similar flux diminution, the non-controlling steps PFK-1, PYK or TPI in AS-30D glycolysis needed to be inhibited by 71%, 99.2% and 99.5%, respectively (Fig. 3A). Interestingly, 50% inhibition of flux (or ATP concentration) was attained, in AS-30D glycolysis, when GLUT + HK or GLUT + HK + HPI were decreased simultaneously by the same magnitude, 63% and 47% inhibition, respectively, whereas in HeLa glycolysis, when GLUT + glycogen degradation were decreased simultaneously by 48% (Fig. 3B).

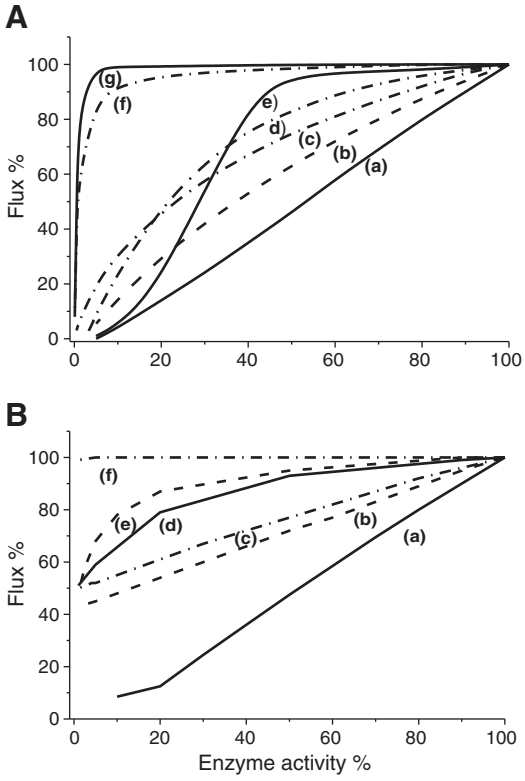

Fig. 3. Dependence of tumor glycolytic flux on enzyme activity. The reference 100% enzyme activity values were those corresponding to the respective *Vm* values for the forward reaction (Tables 1 and S3) whereas 100% fluxes were those predicted by each model (A for AS-30D; B for HeLa cells), which were the fluxes through LDH (29 and 20 nmol min^{-1} (mg cell protein)$^{-1}$, respectively; Tables 3 and 4). In A, enzymes, transporters and braches were (a) GLUT + HK + HPI; (b) GLUT + HK; (c) HK or HPI; (d)GLUT; (e) PFK-1; (f) PYK and (g)TPI. In B, (a) GLUT + glycogen degradation; (b) glycogen degradation; (c) GLUT; (d) HK; (e) HPI and (f) TPI. When two or more steps were titrated, identical variation in activity was applied. A decrease of the Vm_f value was accompanied by a proportional decrease in the Vm_r value.

4. Concluding remarks

The kinetic models for both tumor cells predicted reasonably well fluxes and metabolite concentrations found in living cells. To achieve high robustness, the models were built up with the kinetic properties of each individual enzyme determined experimentally including (a) the most common ligands (substrates, products and modulators), and (b) the interactions of several other pathway intermediaries with the enzymes (Fig. 1). Also, the great majority of the changes made to improve and refine the models were based on "wet" experimentation. This allowed us to identify some mechanisms by which a traditionally considered non-controlling enzyme such as HPI may exert significant control on tumor glycolysis. However, further rounds of model refinement are still necessary to reach more prediction accuracy, especially for F6P and PEP concentrations. Nevertheless, the present models may serve to predict the pathway behavior under other physiological conditions and in other cancer cell lines as long as the most controlling steps are experimentally evaluated.

Thus, kinetic modeling is a helpful theoretical–experimental approach to identifying the most promising therapeutic targets. It has been proposed that inhibition of glycolysis in tumor cells can be an alternative therapeutic strategy [6,61] and several therapeutic targets have been proposed (GLUT1, HKII, PFKFB3, GAPDH, LDH, and MCT) [37, reviewed in 62–65]. It then results of clinical relevance to experimentally evaluate whether such targets are indeed flux control steps of the tumor cells' pathway. Moreover, it would be desirable that such targets have high flux control in tumor cells, but low control in host, normal cells.

In normal cells, HK and PFK-1, together with GLUT, exert the main control on the glycolytic flux [reviewed in 8]. However, due to the different enzyme activity levels, different control distribution was expected, and demonstrated here, between HeLa (glycogen degradation ≥ GLUT > HK) and AS-30D (HK ≥ HPI > GLUT) cells; and between these and normal cells: PFK-1 played a minor role on flux- and metabolite-control in cancer cells, except for the hypoxia condition. The main flux-controlling steps are the targets with the higher potential to diminish the glycolytic flux in the two cancer cells examined. Although the glycogen degradation pathway was a high controlling step in HeLa glycolysis, it could not be an appropriate drug target because glycogen degradation cannot be sustained by prolonged periods of time.

In summary, drug-design studies targeting the most controlling enzymes or transporters in tumor glycolysis might have more promissory results than targeting non-controlling enzymes which usually require more potent and specific inhibitors to accomplish the required full inhibition to achieving effect on function. Another

strategy would be that of a multi-targeted therapy against the most controlling steps as previously suggested [*cf*. Fig. 3; see also 9].

From a therapeutic point of view, the kinetic models are useful for predicting how pathway fluxes and ATP concentration may vary when one or more steps are inhibited. The results of the simulations indicated that only the simultaneous inhibition of the controlling steps may have significant impact on glycolytic flux and ATP concentration. Other interventions such as inhibition of solely one controlling step, or worse, of non-controlling steps will bring about negligible effects on pathway behavior. For the latter, their negligible flux-control coefficients demand the design of highly potent and very specific inhibitors for the tumor steps or their full gene transcription or translation blockade.

Supplementary materials related to this article can be found online at doi:10.1016/j.bbabio.2010.11.006.

Acknowledgements

This research was supported by CONACyT-México grants No. 80534 and 123636 to RMS and 83084 to ES, and Instituto de Ciencia y Tecnologia del Distrito Federal grant No. PICS08-5. AMH was supported by a CONACyT fellowship (No. 59991).

References

[1] R. Moreno-Sánchez, S. Rodríguez-Enríquez, A. Marín-Hernández, E. Saavedra, Energy metabolism in tumor cells, FEBS J. 274 (2007) 1393–1418.
[2] R. Moreno-Sánchez, S. Rodríguez-Enríquez, E. Saavedra, A. Marín-Hernández, J.C. Gallardo-Pérez, The bioenergetics of cancer: is glycolysis the main ATP supplier in all tumor cells? Biofactors 35 (2009) 209–225.
[3] C.V. Dang, J.W. Kim, P. Gao, J. Yustein, The interplay between MYC and HIF in cancer, Nat. Rev. Cancer 8 (2008) 51–56.
[4] S.J. Yeung, J. Pan, M.H. Lee, Roles of p53, Myc and HIF-1 in regulating glycolysis—the seventh hallmark of cancer, Cell. Mol. Life Sci. 65 (2008) 3981–3999.
[5] A. Marín-Hernández, J.C. Gallardo-Pérez, S.J. Ralph, S. Rodríguez-Enríquez, R. Moreno-Sánchez, HIF-1α modulates energy metabolism in cancer cells by inducing over-expression of specific glycolytic isoforms, Mini Rev. Med. Chem. 9 (2009) 1084–1101.
[6] S. Rodríguez-Enríquez, A. Marín-Hernández, J.C. Gallardo-Pérez, L. Carreño-Fuentes, R. Moreno-Sánchez, Targeting of cancer energy metabolism, Mol. Nutr. Food Res. 53 (2009) 29–48.
[7] D. Fell, Understanding the Control of Metabolism, Portland Press, London, 1997.
[8] R. Moreno-Sánchez, E. Saavedra, S. Rodríguez-Enríquez, V. Olín-Sandoval, Metabolic control analysis: a tool for designing strategies to manipulate pathways, J. Biomed. Biotech. 2008 (2008) 597913.
[9] R. Moreno-Sánchez, E. Saavedra, S. Rodríguez-Enríquez, J.C. Gallardo-Pérez, H. Quezada, H.V. Westerhoff, Metabolic control analysis indicates a change of strategy in the treatment of cancer, Mitochondrion 10 (2010) 626–639.
[10] A. Marín-Hernández, S. Rodríguez-Enríquez, P.A. Vital-González, F.L. Flores-Rodríguez, M. Macias-Silva, M. Sosa-Garrocho, R. Moreno-Sánchez, Determining and understanding the control of glycolysis in fast-growth tumor cells. Flux control by an over-expressed but strongly product-inhibited hexokinase, FEBS J. 273 (2006) 1975–1988.
[11] J.L. Snoep, The silicon cell initiative: working towards a detailed kinetic description at the cellular level, Curr. Opin. Biotechnol. 16 (2005) 336–343.
[12] J.J. Hornberg, F.J. Bruggeman, B.M. Bakker, H.V. Westerhoff, Metabolic control analysis to identify optimal drug targets, Prog. Drug Res. 64 (2007) 173–189.
[13] E. Saavedra, R. Encalada, E. Pineda, R. Jasso-Chávez, R. Moreno-Sánchez, Glycolysis in *Entamoeba histolytica*. Biochemical characterization of recombinant glycolytic enzymes and flux control analysis, FEBS J. 272 (2005) 1767–1783.
[14] E. van Schaftingen, B. Lederer, R. Bartrons, H.G. Hers, A kinetic study of pyrophosphate: fructose-6-phosphate phosphotransferase from potato tubers, Eur. J. Biochem. 129 (1982) 191–195.
[15] H.U. Bergmeyer, Methods of Enzymatic Analysis, Verlag Chemie, Winheim, 1983.
[16] E. Saavedra, A. Marín-Hernández, R. Encalada, A. Olivos, G. Mendoza-Hernández, R. Moreno-Sánchez, Kinetic modeling can describe in vivo glycolysis in *Entamoeba histolytica*, FEBS J. 274 (2007) 4922–4940.
[17] P.C. Heinrich, H.P. Morris, G. Weber, Behavior of transaldolase and transketolase activities in normal, neoplastic, differentiating and regenerating liver, Cancer Res. 36 (1976) 3189–3197.
[18] S. Rodríguez-Enríquez, P. Vital-Gónzalez, F.L. Flores-Rodríguez, A. Marín-Hernández, L. Ruiz-Ramírez, R. Moreno-Sánchez, Control of cellular proliferation by modulation of oxidative phosphorylation in human and rodent fast-growing tumor cells, Toxicol. Appl. Pharmacol. 215 (2006) 208–217.
[19] S. Rodriguez-Enriquez, L. Carreño-Fuentes, J.C. Gallardo-Pérez, E. Saavedra, H. Quezada, A. Vega, A. Marín-Hernández, V. Olín-Sandoval, M.E. Torres-Márquez, R. Moreno-Sánchez, Oxidative phosphorylation is impaired by prolonged hypoxia in breast but not in cervix carcinoma, Int. J. Biochem. Cell Biol. 42 (2010) 1744–1751.
[20] H.U. Bergmeyer, Methods of Enzymatic Analysis, Weinheim, Verlag Chemie, 1974.
[21] E.S. Baginski, P.P. Foà, B. Zak, Microdetermination of inorganic phosphate, phospholipids, and total phosphate in biologic materials, Clin. Chem. 12 (1967) 326–332.
[22] T.P.M. Akerboom, H. Bookelman, P.F. Zuurendonk, R. Meer, J.M. Tager, Intramitochondrial and extramitochondrial concentrations of adenine nucleotides and inorganic phosphate in isolated hepatocytes from fasted rats, Eur. J. Biochem. 84 (1978) 413–420.
[23] P. Mendes, GEPASI: a software package for modeling the dynamics, steady states and control of biochemical and other systems, Comput. Appl. Biosci. 9 (1993) 563–571.
[24] S. Rodríguez-Enríquez, A. Marín-Hernández, J.C. Gallardo-Pérez, R. Moreno-Sánchez, Kinetics of transport and phosphorylation of glucose in cancer cells, J. Cell. Physiol. 221 (2009) 552–559.
[25] I.H. Segel, Enzyme Kinetics, Wiley, New York, 1975.
[26] T. Rapoport, R. Heinrich, G. Jacobasch, S. Rapoport, A mathematical model of glycolysis of human erythrocytes, Eur. J. Biochem. 42 (1974) 107–120.
[27] F.B. du Preez, R. Conradie, G.P. Penkler, K. Holm, F.L.J. van Dooren, J.L. Snoep, A comparative analysis of kinetic models of erythrocyte glycolysis, J. Theor. Biol. 252 (2008) 488–496.
[28] B. Teusink, J. Passarge, C.A. Reijenga, E. Esgalhado, C.C. van der Weijden, M. Schepper, M.C. Walsh, B.M. Bakker, K. van Dam, H.V. Westerhoff, J.L. Snoep, Can yeast glycolysis be understood in terms of in vitro kinetics of the constituent enzymes? Testing biochemistry, Eur. J. Biochem. 267 (2000) 5313–5329.
[29] B.M. Bakker, M.C. Walsh, B.H. Ter Kuile, F.I.C. Mensonides, P.A.M. Michels, F.R. Opperdoes, H.V. Westerhoff, Contribution of glucose transport to the control of the glycolytic flux in *Trypanosoma brucei*, Proc. Natl Acad. Sci. USA 96 (1999) 10098–10103.
[30] S. Rodríguez-Enríquez, O. Juárez, J.S. Rodríguez-Zavala, R. Moreno-Sánchez, Multisite control of the Crabtree effect in ascites hepatoma cells, Eur. J. Biochem. 268 (2001) 2512–2519.
[31] R. Wu, Regulatory mechanisms in carbohydrate metabolism. V. Limiting factors of glycolysis in HeLa cells, J. Biol. Chem. 234 (1959) 2806–2810.
[32] R. Nakashima, M. Paggi, L.J. Scott, P.L. Pedersen, Purification and characterization of a bindable form of mitochondrial bound hexokinase from the highly glycolytic AS-30D rat hepatoma cell line, Cancer Res. 48 (1988) 913–919.
[33] D.M. Parry, P.L. Pedersen, Intracellular localization and properties of particulate hexokinase in the Novikoff ascites tumor, J. Biol. Chem. 258 (1983) 10904–10912.
[34] K.K. Arora, P.L. Pedersen, Functional significance of mitochondrial bound hexokinase in tumor cell metabolism, J. Biol. Chem. 263 (1988) 17422–17428.
[35] G.E.J. Staal, A. Kalff, E.C. Hessbeen, C.W.M. van Veelen, G. Rijksen, Subunit composition, regulatory properties and phosphorylation of phosphofructokinase from human gliomas, Cancer Res. 47 (1987) 5047–5051.
[36] L.J. Mandarino, R.L. Printz, K.A. Cusi, P. Kinchington, R.M. O'Doherty, H. Osawa, C. Sewell, A. Consoli, D.K. Granner, R.A. Defronzo, Regulation of hexokinase II and glycogen synthase mRNA, protein, and activity in human muscle, Am. J. Physiol. 269 (1995) E701–E708.
[37] S. Kumagai, R. Narasaki, K. Hasumi, Glucose-dependent active ATP depletion by koningic acid kills high-glycolytic cells, Biochem. Biophys. Res. Commun. 365 (2008) 362–368.
[38] S. Rodríguez-Enríquez, M.E. Torres-Márquez, R. Moreno-Sánchez, Substrate oxidation and ATP supply in AS-30D hepatoma cells, Arch. Biochem. Biophys. 375 (2000) 21–30.
[39] L.J. Reitzer, B.M. Wice, D. Kennell, The pentose cycle, J. Biol. Chem. 255 (1980) 5616–5626.
[40] K.A. Gumaa, P. McLean, The pentose phosphate pathway of glucose metabolism, Biochem. J. 115 (1969) 1009–1029.
[41] J.C. Portais, R. Schuster, M. Merle, P. Canioni, Metabolic flux determination in C6 glioma cells using carbon-13 distribution upon [1-^{13}C] glucose incubation, Eur. J. Biochem. 217 (1993) 457–468.
[42] C.M. Metallo, J.L. Walter, G. Stephanopoulos, Evaluation of ^{13}C isotopic tracers for metabolic flux analysis in mammalian cells, J. Biotechnol. 144 (2009) 167–174.
[43] J.W. Harding, E.A. Pyeritz, H.P. Morris, H.B. White, Proportional activities of glycerol kinase and glycerol 3-phosphate dehydrogenase in rat hepatomas, Biochem. J. 148 (1975) 545–550.
[44] B.W. Agranoff, A.K. Hajra, The acyl dihydroacetone phosphate pathway for glycerolipid biosynthesis in mouse liver and Ehrlich ascites tumor cells, Proc. Natl Acad. Sci. USA 68 (1971) 411–415.
[45] K. Snell, G. Weber, Enzymic imbalance in serine metabolism in rat hepatomas, Biochem. J. 233 (1986) 617–620.
[46] G. Paradies, F. Capuano, G. Palombini, T. Galeotti, S. Papa, Transport of pyruvate in mitochondria from different tumor cells, Cancer Res. 43 (1983) 5068–5071.
[47] S.J. Ralph, S. Rodríguez-Enríquez, J. Neuzil, R. Moreno-Sánchez, Bioenergetic pathways in tumor mitochondria as targets for cancer therapy and the importance of the ROS-induced apoptotic trigger, Mol. Aspects Med. 31 (2010) 29–59.
[48] J. Zalitis, I.T. Oliver, Inhibition of glucose phosphate isomerase by metabolic intermediates of fructose, Biochem. J. 102 (1967) 753–759.
[49] J.M. Chirgwin, T.F. Parsons, A.N. Ernst, Mechanistic implications of the pH independence of inhibition of phosphoglucose isomerase by neutral sugar phosphates, J. Biol. Chem. 250 (1975) 7277–7279.
[50] M.K. Gaitonde, E. Murray, V.J. Cunningham, Effect of 6-phosphogluconate on phosphoglucose isomerase in rat brain in vitro and in vivo, J. Neurochem. 52 (1989) 1348–1352.
[51] F. Heinz, K.D. Kulbe, Glyceraldehyde phosphate dehydrogenase from liver: I. Isolation and characterization of the bovine liver enzyme, Hoppe Seylers, Z. Physiol. Chem. 351 (1970) 249–261.

[52] S. Patra, S. Ghosh, S. Bera, A. Roy, S. Ray, M. Ray, Molecular characterization of tumor associated glyceraldehyde-3-phosphate dehydrogenase, Biochemistry (Mosc) 74 (2009) 717–727.
[53] A. Tanaka, B. Chance, B. Quistorff, A possible role of inorganic phosphate as a regulator of oxidative phosphorylation in combined urea synthesis and gluconeogenesis in perfused rat liver, J. Biol. Chem. 264 (1989) 10034–10040.
[54] L. Nascimben, J.S. Ingwall, B.H. Lorell, I. Pinz, V. Schultz, K. Tornheim, R. Tian, Mechanism for increased glycolysis in the hypertrophied rat heart, Hypertension 44 (2004) 662–667.
[55] B. Teusink, M.C. Walsh, K. van Dam, H.V. Westerhoff, The danger of metabolic pathways with turbo design, Trends Biochem. Sci. 23 (1998) 162–169.
[56] Y.K. Kashiwaya, K. Sato, N. Tsuchiya, S. Thomas, D.A. Fell, R.L. Veech, J.V. Passonneau, Control of glucose utilization in working perfused rat heart, J. Biol. Chem. 269 (1994) 25502–25514.
[57] R. Moreno-Sánchez, R. Encalada, A. Marín-Hernández, E. Saavedra, Experimental validation of metabolic pathway modeling. An illustration with glycolytic segments from *Entamoeba histolytica*, FEBS J. 275 (2008) 3454–3469.
[58] S. Aiston, B. Andersen, L. Agius, Glucose 6-phosphate regulates hepatic glycogenolysis through inactivation of phosphorylase, Diabetes 52 (2003) 1333–1339.
[59] H. Yun, M. Lee, S.-S. Kim, J. Ha, Glucose deprivation increases mRNA stability of vascular endothelial growth factor through activation of AMP-activated protein kinase in DU145 prostate carcinoma, J. Biol. Chem. 280 (2005) 9963–9972.
[60] M. Natsuizaka, M. Ozasa, S. Darmanin, M. Miyamoto, S. Kondo, S. Kamada, M. Shindoh, F. Higashino, W. Suhara, H. Koide, K. Aita, K. Nakagawa, T. Kondo, M. Asaka, F. Okada, M. Kobayashi, Synergistic up-regulation of hexokinase-2, glucose transporters and angiogenic factors in pancreatic cancer cells by glucose deprivation and hypoxia, Exp. Cell Res. 313 (2007) 3337–3348.
[61] H. Pelicano, D.S. Martin, R.H. Xu, P. Huang, Glycolysis inhibition for anticancer treatment, Oncogene 25 (2006) 4633–4646.
[62] P.L. Pedersen, S. Mathupala, A. Rempel, J.F. Geschwind, Y.H. Ko, Mitochondrial bound type II hexokinase; a key player in the growth and survival of many cancers and an ideal prospect for therapeutic intervention, Biochim. Biophys. Acta 1555 (2002) 14–20.
[63] M.L. Macheda, S. Rogers, J.D. Best, Molecular and cellular regulation of glucose transporter (GLUT) proteins in cancer, J. Cell. Physiol. 202 (2005) 654–662.
[64] S.P. Mathupala, C.B. Colen, P. Parajuli, A.E. Sloan, Lactate and malignant tumors: a therapeutic target at the stage of glycolysis, J. Bioenerg. Biomembr. 39 (2007) 73–77.
[65] A. Yalcin, S. Telang, B. Clem, J. Chesney, Regulation of glucose metabolism by 6-phosphofructo-2-kinase/fructose-2, 6-bisphosphatases, Exp. Mol. Pathol. 86 (2009) 174–179.
[66] J.E. Wilson, Isozymes of mammalian hexokinase: structure, subcellular localization and metabolic function, J. Exp. Biol. 206 (2003) 2049–2057.